https://doi.org/10.1016/j.jmmm.2024.171785

Tunable compensation temperature through ferromagnetic coupling in perpendicular $Tb_3Fe_5O_{12}/Eu_3Fe_5O_{12}$ bilayer heterostructure

Pei Gen Li,[1] Jing Ming Liang,[1] Sheung Mei Ng,[1] Hon Fai Wong,[1] Yan Zhou,[2] Ling Jhen Huang,[3] Ko Wei Lin,[3] Yuen Hong Tsang,[1] Chee Leung Mak,[1] and Chi Wah Leung[1,a)]

[1]Department of Applied Physics, The Hong Kong Polytechnic University, Hung Hom, Hong Kong, China

[2]School of Science and Engineering, Chinese University of Hong Kong, Shenzhen, Guangdong 518172, China

[3]Department of Materials Sciences and Engineering, National Chung Hsing University, Taichung 40227, Taiwan

[a)]Author to whom correspondence should be addressed: dennis.leung@polyu.edu.hk

Abstract

Rare-earth ion garnets (ReIG) with magnetization compensation are being extensively studied, such as in the ferrimagnetic insulator (FMI)/heavy metal (HM) heterostructures, with primary focus on the interface effect between single-layer garnets and HM. Here, we study the anomalous Hall behavior of bilayer garnet in $Tb_3Fe_5O_{12}$ (TbIG)/$Eu_3Fe_5O_{12}$ (EuIG)/Pt system. TbIG (30 nm)/EuIG (t nm) films with strong perpendicular magnetic anisotropy (PMA) were deposited on single-crystal $Gd_3Ga_5O_{12}$ (GGG) (111) substrates using pulsed laser deposition. Subsequently, a 5 nm layer of Pt was sputtered and patterned into Hall bars. Tunable compensation temperature (T_{comp}) was achieved in the system by changing the thickness of EuIG, which is ascribed to the ferromagnetic coupling of Fe sublattices in the two different garnets. This study provides guidance for designing garnet spintronic devices with controllable compensation behavior.

Keywords: iron garnet, magnetization compensation, perpendicular magnetic anisotropy, spin Hall effect

1. Introduction

Rare-earth (Re) ion garnets (ReIG) films are heavily studied in the ferromagnetic insulator (FMI)/heavy metal (HM) systems, of which the most well-known is $Y_3Fe_5O_{12}$ (YIG)/Pt [1-5]. Much effort was made into exploring phenomena such as the spin pumping effect [6, 7] spin-Hall effect [8-10], inverse spin-Hall effect [1, 11], and spin Seebeck effect [12, 13] in these systems. Meanwhile, due to the strong temperature dependence of magnetization in Re ions (like Tb, Gd, Dy, etc.) and antiparallel alignment of Fe^{3+} moments in ReIG, some ReIGs show magnetization compensation at certain temperatures (T_{comp}) where the saturation magnetization temporarily vanishes [14-19].

For ReIG with perpendicular magnetic anisotropy (PMA), hysteretic behaviour can be observed through the anomalous Hall effect resistance (R_{AHE}) of the corresponding FMI/HM system, and recent studies attempted to explain the phenomena [16, 20-22]. Advanced technologies like polarized neutron reflectivity and X-ray circular dichroism are used to study the magnetic proximity behavior of the FMI/HM interface and the coupling between sublattices [20], revealing the competitive relationships of sublattices magnetism around T_{comp}.

Previous studies on ReIG/HM have identified various phenomena associated with the magnetization compensation behaviors in ReIG, including temperature dependence of R_{AHE} ReIG/HM across T_{comp}, interfacial modification in ReIG/HM system to regulate the spin-Hall magnetotransport [20], or the relation between T_{comp} with the thickness of single-layer ReIG film [23]. Particularly, two sign reversals in hysteretic R_{AHE} with changing temperatures can be observed in ReIG/Pt with ReIG possessing compensation points. In TbIG/Pt for example, the sign reversal around 220 K coincides with the T_{comp} of TbIG [14, 24, 25]. Similar T_{comp} phenomenon is also observed in DyIG/Pt and GdIG/Pt [18, 26]. The second R_{AHE} sign reversal occurs typically at temperatures below T_{comp}, and is suggested to arise from the competition between the magnetic proximity effect (MPE) induced in the Pt layer and the spin Hall (SH) magnetotransport at the interface [20, 27, 28].

Relatively little attention is paid to multilayers composed of different ReIG materials. Some studies were made on exploring the spin-Hall transport behavior by constructing trilayer structures with an antiferromagnetic spacer (e.g. NiO) sandwiched between two ReIG layers,

forming the so-called magnon valves [29, 30]. The large lattice mismatch between NiO and ReIG systems leads to differences in the crystallinity of top and bottom garnet layers, and all-ReIG systems with similar crystal structures can avoid these issues. The impact of the ReIG materials in close proximity on the magnetic and spin magnetotransport behaviour is worth exploring.

In this work, we demonstrate the adjustable extrinsic magnetic compensation point by constructing bilayer garnet films (TbIG and EuIG). While the compensation point is an intrinsic property of some garnets like TbIG, independent of additional magnetic moments, the modulation of extrinsic magnetization compensation in iron garnet films can be achieved by constructing ReIG bilayers composed of two different garnets. This extrinsic compensation behavior originates from the combined magnetic contributions of different layers. Here, the bottom TbIG has fixed thickness, the top EuIG layer thickness is varied to study the impact on the spin-Hall transport behaviour in the topmost Pt layer. Particular attention is paid to the effect of lattice-matching EuIG insertion on the R_{AHE} behavior in the Pt layer as compared to the control TbIG/Pt sample. EuIG has a garnet structure with lattice constant (a_{EuIG} = 12.500 Å) [31] similar to that of TbIG (a_{TbIG} =12.436 Å) [32] and $Gd_3Ga_5O_{12}$ (GGG) (a_{GGG} = 12.376 Å) [31], the latter of which is commonly used for epitaxial growth of ReIG thin films. Specially, GGG(111)/TbIG and GGG(111)/EuIG can maintain the PMA because of the in-plane compressive strain and positive magnetostrictive constants in [111] direction [33]. Besides, EuIG alone does not exhibit magnetization compensation [34], making it a suitable candidate to explore the impact on TbIG/Pt through observing magnetization compensation regulation in the heterostructures. The temperature dependence of anomalous Hall resistance (R_{AHE}) was measured on the samples to probe the T_{comp}. The experimental results indicate that extrinsic T_{comp} can be tuned in the TbIG/EuIG system through varying the EuIG thickness, and the interface coupling situation at TbIG/EuIG was discussed.

2. Experimental Details

For film and device fabrication, TbIG (30 nm)/EuIG (t nm) (with t ranging between 0 to 20 nm) were deposited on GGG (111) substrates by pulsed laser deposition (PLD). The films were grown at 710 °C in an oxygen ambient of 100 mTorr, using a KrF excimer laser with a

wavelength of λ=248 nm, pulses energy of 340 J, and a repetition rate of 2 Hz. The deposition sequence is shown in Fig. 1(a). Before deposition, substrates were annealed in air at 1000 ºC for 6 hours to produce a reconstructed GGG surface, promoting the smooth growth of the films [14]. After deposition, 5 nm of Pt was deposited *ex-situ* by d.c. magnetron sputtering and subsequently patterned into Hall bars using photolithography and broad-beam ion milling. The specific thickness was measured through the high-resolution transmission electron microscope (HRTEM) image and found to be approximately 30 nm (see Figs. S1), which matches the value we calibrated using calibration sample.

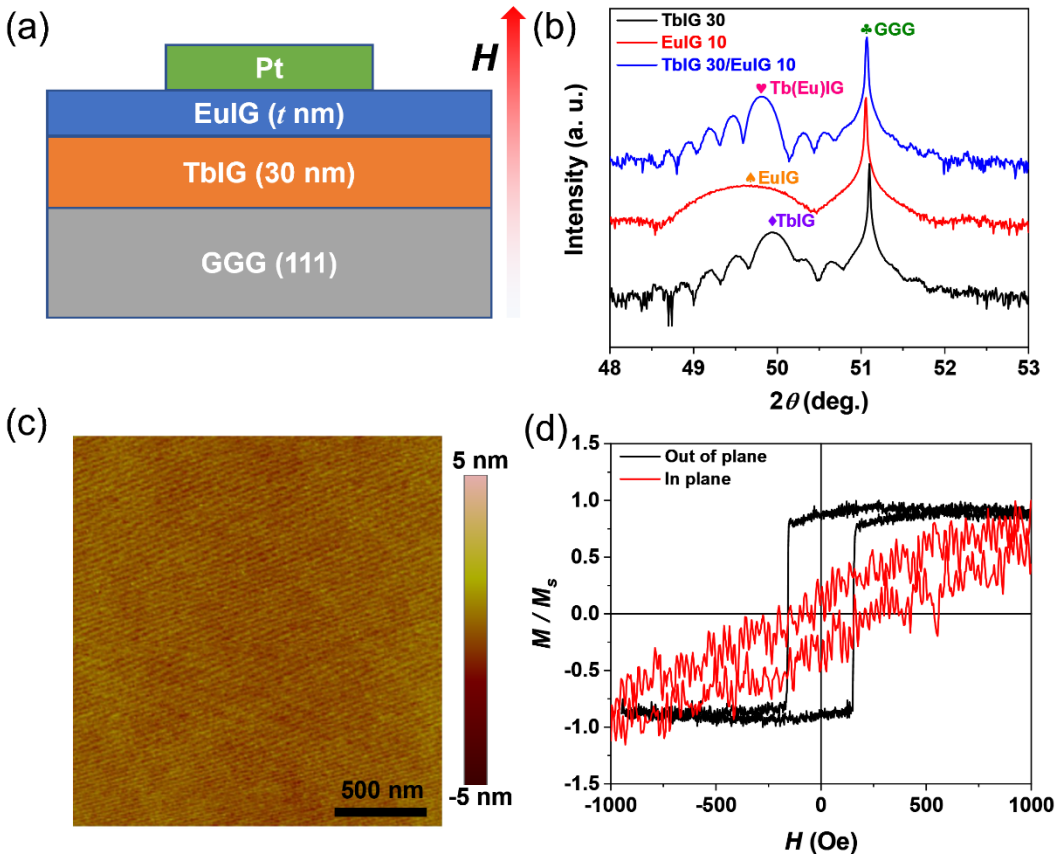

Fig. 1. (a) Schematic illustration of TbIG/EuIG/Pt device. (b) XRD diffraction profile of single-layer TbIG (30 nm) and EuIG (10 nm), and the TbIG (30 nm)/EuIG (10 nm) bilayer. (c) AFM image of GGG/TbIG (30 nm)/EuIG (10 nm) film. (d) In-plane (red) and out-of-plane (black) normalized *M-H* hysteresis loops of TbIG (30 nm)/EuIG (10 nm) at room temperature as measured by VSM.

High-resolution X-ray diffractometry (XRD, Rigaku SmartLab) was used to characterize

the microstructure of TbIG/EuIG bilayers. The surface morphology was probed using atomic force microscopy (AFM, Asylum 3D infinity). Transmission electron microscopy (TEM, JEM-F200) equipped with high-angle annular dark field (HAADF) and EDX mappings were used for inspecting the crystallinity and elemental distribution, with the specimen prepared by focused ion beam microscopy (FIB, Helios 5 UX). Magnetic hysteresis loops were measured by a vibrating sample magnetometer (VSM, Lakeshore). Magnetotransport properties were measured by a physical property measurement system (PPMS, Quantum Design). R_{AHE} were detected from the samples with external magnetic field applied perpendicular to the substrates.

3. Results and Discussion

Fig. 1(b) shows the X-ray 2θ scan of single layer TbIG(30 nm) and EuIG(10 nm) films, as well as TbIG (30 nm)/EuIG (10 nm) bilayers. In addition to the sharp GGG (444) substrate peak, the EuIG peak is observed at $2\theta = 49.61°$ and is lower than the TbIG peak ($2\theta = 49.93°$). As both the lattice parameters of EuIG and TbIG are larger than that of GGG, all films show in-plane compressive strain, and EuIG peak is shifted towards lower 2θ value due to the larger lattice size. For the bilayer sample, the combined peak position at $2\theta = 49.81°$ is between that of single-layered EuIG and TbIG. The actual thickness of TbIG (30 nm)/EuIG (10 nm) bilayer sample can be confirmed by the TEM image (Fig. S1 in Supporting Information), which is consistent with our expected thickness. Epitaxial relationship between the films and the substrate can be evidenced from the phi scan (see Figs. S1 and S2). The surface morphology was probed using AFM. Fig. 1(c) presents the surface morphology of GGG/TbIG (30 nm)/EuIG (10 nm) sample. The root-mean-square roughness of 0.34 nm indicates an atomically smooth sample surface.

PMA in ReIG facilitates the observation of hysteretic AHE signals and spin-orbit torque-based magnetization reversal in ReIG/Pt systems [24, 35]. Previous studies showed that single-layer EuIG and TbIG thin films on GGG (111) substrates exhibit out-of-plane easy axis [14, 36, 37]. To verify that PMA is retained in the ReIG bilayers, in-plane and out-of-plane magnetic hysteresis loops of TbIG (30 nm)/EuIG (10 nm) film were measured by VSM at room temperature. As shown in Fig. 1(d), the out-of-plane *M-H* shows a squared loop, indicating the

easy axis of the bilayer is along the sample normal direction.

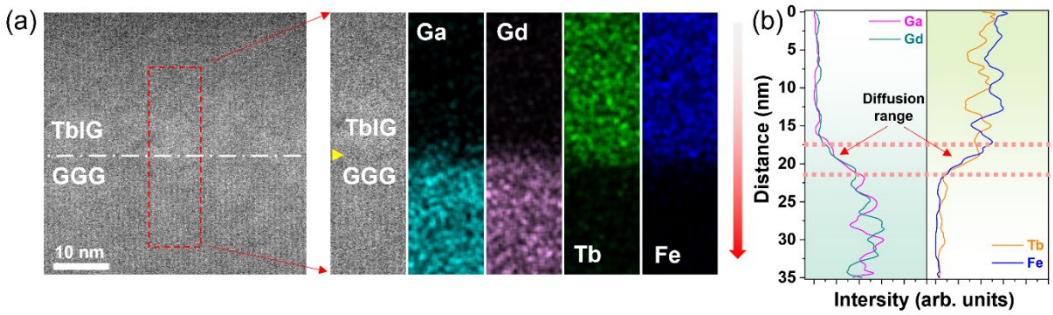

Fig. 2. (a) STEM image of the GGG/TbIG interface. The red dashed rectangle range was extracted for EDX mapping analysis. (b) The average signal intensity of different elements (Ga, Gd, Tb, and Fe) was obtained from the line scan.

Fig. 2 displays STEM and the energy-dispersive x-ray spectroscopy (EDX) images across the GGG/TbIG interface. The STEM image in Fig. 2(a) shows a highly crystallized and flat GGG/TbIG interface, consistent with the XRD and AFM results in Figs. 1(b) and 1(c). EDX element distribution analysis was conducted in selected region of Fig. 2(a). The distribution of various elements (Ga, Gd, Tb, and Fe) in Fig. 2(a) indicates diffusion across the interface. Line scan analysis results [Fig. 2(b)] suggest an interdiffusion range of around 4 nm across the substrate/film interface. Such transient layer is commonly observed in ReIG films [38-40]. The interdiffusion processes at substrate/garnet interface can generate a continuous composition profile without abrupt changes in the lattice parameters. Cross-sectional TEM (Fig. S1) indicates a change of garnet lattice without detectable dislocations throughout the thickness of the bilayer film. The average lattice plane spacing d_{111} and d_{110} were measured (Fig. S3). Due to the small lattice mismatch (0.48%) between GGG and TbIG, d_{111} and d_{110} show no obvious change and are close to that of GGG substrate. While the thickness of the transient layer at GGG/TbIG interface depends on the deposition parameters, it is justified to assume that being constant in our bilayer samples, and the impact on the magnetization and T_{comp} on all TbIG/EuIG samples should be identical.

While the majority of previous studies focused on MPE or spin-Hall transport at the interface of ReIG/Pt [14, 37], little attention was paid on the influence of an adjacent iron garnet layer with different Re composition (ReIG') on an existing ReIG/Pt system. In this study, we

placed EuIG of different thicknesses in proximity with Pt, while a TbIG (30 nm) layer serves as the adjacent ReIG', forming a multilayer stack of TbIG(30 nm)/EuIG (*t* nm)/Pt.

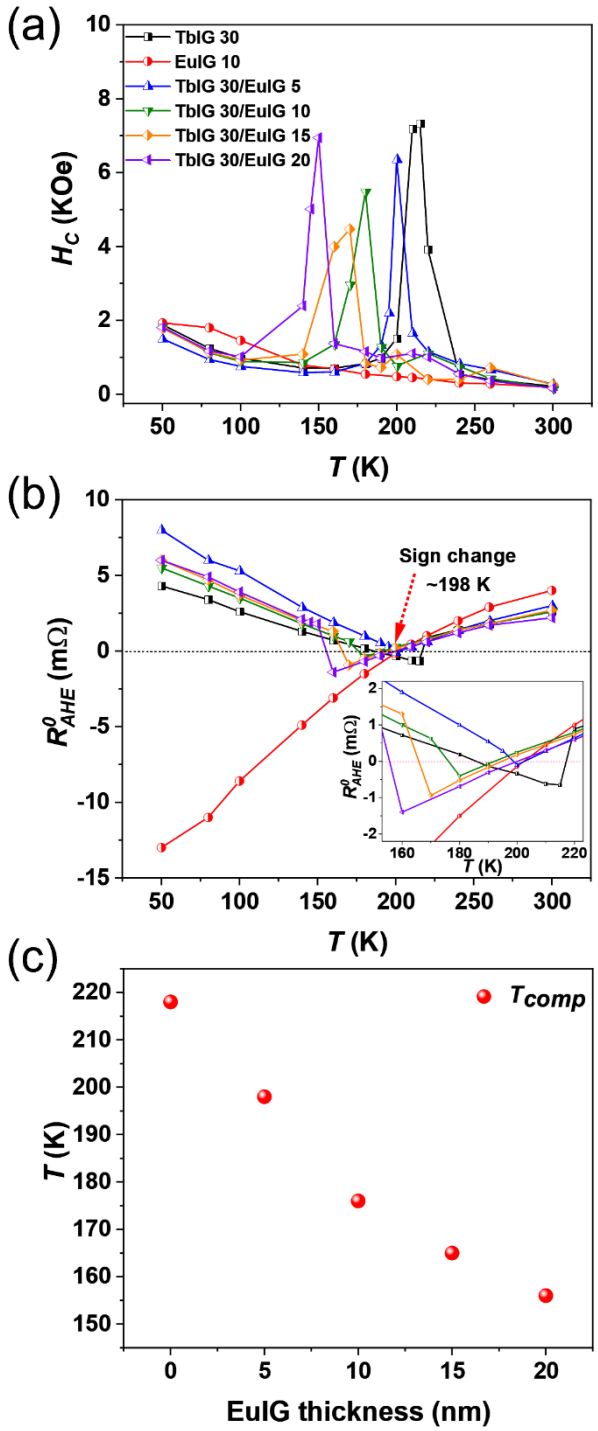

Fig. 3. Temperature dependence of (a) H_c and (b) R^0_{AHE}. All H_c and R^0_{AHE} were obtained from the R_{AHE}-H loops at corresponding temperatures. The inset in (b) shows the amplified part of the R^0_{AHE}-T around R^0_{AHE} cross-over. (c) EuIG thickness dependent T_{comp}.

R_{AHE}-H loops of the samples at various temperatures are plotted in Figs. S4-S9 of Supporting Information, and the corresponding H_c (as extracted at $R_{AHE} = 0$) and R_{AHE} at zero fields (R_{AHE}^0) are shown in Figs. 3(a) and 3(b). Divergence of H_c can be observed from Fig. 3(a). Both Tb^{3+} and Fe^{3+} in ReIG show temperature dependencies, but Tb^{3+} decays more rapidly and cancel out with Fe^{3+} at around 222 K [23, 41]. As temperature approaches T_{comp}, the magnetization of Tb^{3+} and Fe^{3+} sublattices cancel out, forming a saturation magnetization close to zero and a corresponding H_c divergence due to the decreased Zeeman energy for magnetization reversal [42].

Meanwhile, the T_{comp} greatly affects the spin-Hall transport of ReIG/Pt. As the temperature decreases and passes through T_{comp}, Tb^{3+} replaces Fe^{3+} and dominates the overall magnetization, while the two types of ions remain antiparallel. Meanwhile, it is known that Fe-Pt coupling determines the spin-Hall magnetotransport behavior [20]. A cross-over at T_{comp} therefore leads to an abrupt R_{AHE}^0 sign reversal as Fe^{3+} reorient itself, as evidenced by the rapid R_{AHE}^0 sign change around T_{comp} [inset, Fig. 3(b)]; detailed measurements show that such R_{AHE}^0 sign change can occur within a 5-K temperature interval.

From the above, it can be summarized that both divergent H_c and R_{AHE}^0 sign reversal coincides with T_{comp}. The divergent H_c provides direct evidence for the existence of T_{comp}, the precise identification of which may be difficult due to the exceedingly large fields involved. Meanwhile, R_{AHE}^0 reflects the ReIG/Pt interfacial spin-Hall transport, and its good temperature sensitivity provides a convenient probe for T_{comp} for the ReIG system.

It should be noted that EuIG does not possess T_{comp} in bulk, as supported by the absence of H_c divergence in EuIG (10 nm)/Pt [Fig. 3(a)]. Because the ground state of dodecahedral site Eu^{3+} has total angular momentum $J = 0$ according to Hund's rule, the magnetic contribution of Eu^{3+} to EuIG magnetization can be ignored [34, 43]. In turn, the magnetization of EuIG is solely decided by Fe^{3+} ions, thus ruling out the occurrence of T_{comp} in EuIG. However, H_c divergence is clearly observed among all TbIG/EuIG/Pt samples in Fig. 3(a), and is accompanied by abrupt R_{AHE}^0 sign change at similar temperatures in Fig. 3(b). This suggests a magnetization compensation behavior in the TbIG/EuIG bilayer, similar compensation behavior can be observed in the in-plane YIG/GdIG bilayer system [44].

More importantly, a dependence of such magnetization compensation in TbIG/EuIG with

EuIG thickness can be seen in Figs. 3(a) and 3(b). To this end, T_{comp} was extracted from the R_{AHE}^{0} sign cross-over points for various TbIG/EuIG (t) samples and is plotted in Fig. 3(c). As the thickness of EuIG increases, T_{comp} gradually decreases from 218 K (t = 0 nm) to 156 K (t = 20 nm).

In addition to the cross-over of R_{AHE}^{0} at T_{comp} (which coincides with H_c divergence), another cross-over can be observed at around 198 K [Fig. 3(b)] and is invariant for all samples (including single-layer EuIG). This cross-over is typically attributed to the competition between MPE-induced AHE in the Pt layer and the SH-induced AHE at the ReIG/Pt interface [20]. The magnetic proximity effect is a common phenomenon that induces a magnetic moment in the heavy metal interface when in contact with a magnetic insulator, resulting in limited ferromagnetic ordering in Pt and the production of an AHE signal. Additionally, the spin Hall effect can convert electron current into spin current, and the corresponding inverse spin Hall effect also exists at the FMI/HM interface. The AHE signal, which differs from MPE-induced part, can be activated through the spin current in the heavy metal and shows opposite direction. Because of the different temperature dependence of SH and MPE, at high temperatures, thermal disturbance weakens MPE-induced AHE at EuIG/Pt interface, and the spin current-induced AHE is prevalent. The proximity effect gradually dominates as the temperature decrease, leading to a gradual variation of R_{AHE}^{0} around this cross-over point.

While the competition between MPE-induced AHE and SH-induced AHE has been studied in previous works [20, 28], Fig. 3(b) suggested that the R_{AHE}^{0} sign of single-layer TbIG and EuIG are opposite at the lowest temperatures. As mentioned previously, the magnetization of EuIG is dominated by *d*-site Fe^{3+}, and T_{comp} is not observed in this system; this is reflected in the EuIG/Pt spin-Hall transport measurement, at which R_{AHE}^{0} sign reversal occurs only when MPE-induced AHE and SH-induced AHE cancel out.

However, the R_{AHE}^{0} in TbIG/Pt and TbIG/EuIG/Pt systems show two cross-over of signs with the EuIG thickness studied. As mentioned before, these two reversals follow different mechanisms. As shown in Fig. 3(b), the abrupt R_{AHE}^{0} sign change is accompanied by a divergent H_c and is related to T_{comp}, which shows a strong EuIG thickness dependence [Fig. 3(c)]. This R_{AHE}^{0} sign change originates from the reorientation of Fe^{3+} in ReIG films at T_{comp}. It is known that the antiferromagnetic coupling exists in a-site Fe^{3+}/d-site Fe^{3+} and d-site Fe^{3+}/c-

site Tb^{3+} ions in TbIG, the combined action of different site ions contributes to its intrinsic compensation behavior. The a-site Fe^{3+}/d-site Fe^{3+} sublattices (with *d*-site being dominant among the two) have much stronger exchange coupling (exchange constant $J_{ad} \cong 2.62\ meV$) compared to the Fe^{3+}/Tb^{3+} coupling ($J_{ac} \cong 0.045\ meV$ and $J_{dc} \cong 0.21\ meV$) [45]. Therefore, the net magnetization of TbIG is determined by the Fe^{3+} at above T_{comp}. While the magnetization of Tb^{3+} ions have stronger temperature dependence than Fe^{3+}, the strongly enhanced Fe^{3+}/Tb^{3+} coupling eventually overcomes the magnetic coupling among Fe^{3+}, causing the net magnetization to be dominated by Tb^{3+} at below T_{comp}.

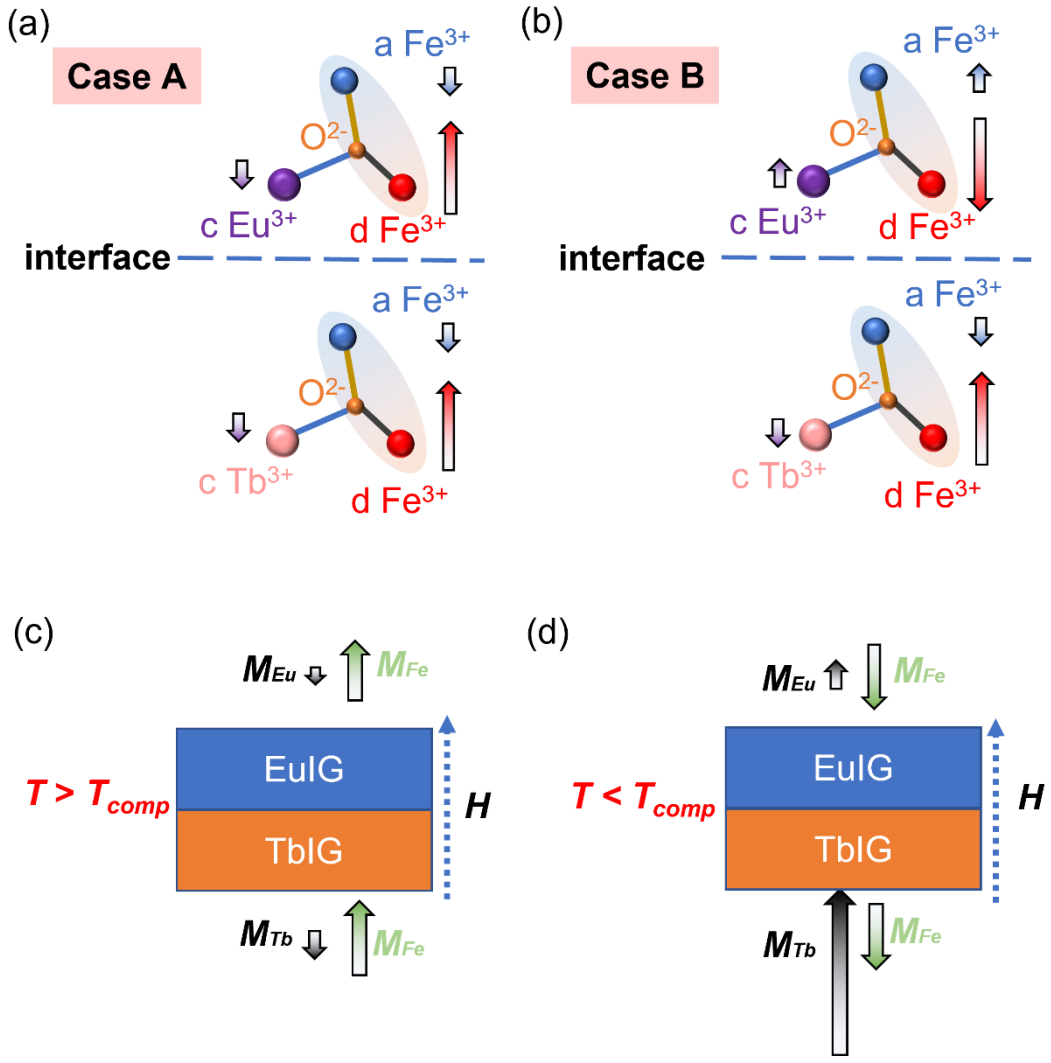

Fig. 4. Possible coupling situations across TbIG/EuIG. (a) Case A model assumes ferromagnetic coupling between Fe_{EuIG} and Fe_{TbIG}, as in contrast with the antiferromagnetic coupling of Fe^{3+} sublattices across the interface in (b) Case B. Schematic illustration of net magnetic moment directions of different elements (c) below and (d) above T_{comp} in the

TbIG/EuIG system.

While the change in T_{comp} could be related to the thickness of the transient layer at the TbIG/EuIG interface. Considering a fixed transient layer because of the same deposition parameters, the value (TbIG/EuIG interface)/(total EuIG thickness) decreases with the increase of the EuIG thickness. The reduced relative thickness leads to a continuous decrease in T_{comp}. The other cross-over point is manifested through a continuous and gentle R_{AHE}^{0} variation with no divergent H_c, and is related to the competition between MPE-induced AHE and SH-induced AHE. As mentioned, this R_{AHE}^{0} sign change occurs at ~ 198 K in all samples.

Interestingly, all the bilayer films still maintain two cross-over points despite the absence of T_{comp} in EuIG. The T_{comp} extracted from the TbIG/EuIG/Pt samples decreases with rising EuIG thickness, indicating that TbIG plays a role in modulating the R_{AHE}^{0} signals as detected from the EuIG/Pt interface, which we argue to arise from the coupling between the EuIG and TbIG layers.

Although the existence of the transient layer at TbIG/EuIG interface may affect the overall magnetic properties, identical conditions are again expected in the bilayers, and the magnetic contribution of Eu^{3+} can be ignored. Based on this, we propose a reasonable theoretical model to explain the trend of T_{comp} change. For the convenience of understanding, we consider the interfacial coupling of the Fe^{3+} sublattices in the EuIG and TbIG layers (Fe_{EuIG} and Fe_{TbIG}) across the TbIG/EuIG interface. Noting that the Fe^{3+} sublattices are formed as a consequence of the antiferromagnetic alignment of *a*-site and *d*-site Fe^{3+} ions. There could be two possible coupling scenarios. Case A (Fig. 4a) shows that the Fe_{TbIG}-Fe_{EuIG} across the TbIG/EuIG interface are ferromagnetically coupled. In Case B [Fig. 4(b)], the interfacial Fe_{TbIG}-Fe_{EuIG} are antiferromagnetically coupled.

To analyse the possibility of the coupling cases, we first discuss the overall magnetization changes at above and below T_{comp}. It is noticed that all the samples show positive R_{AHE}^{0} signs at above T_{comp}, [Fig. 3(b)]. Since at high temperatures both the magnetizations of TbIG and EuIG are dominated by Fe^{3+} sublattices. this results in the overall magnetizations of both EuIG and TbIG pointing toward to the same direction [Fig. 4(c)]. The same R_{AHE}^{0} signs are therefore observed in both TbIG/Pt and TbIG/EuIG/Pt samples. When the temperature drops below T_{comp}, although R_{AHE}^{0} signs reversal occurs in both TbIG/Pt and TbIG/EuIG/Pt samples, the total

magnetization directions of the EuIG and TbIG layer are entirely different. As shown in Fig. 4(d), at tempearatures below T_{comp}, the magnetization of EuIG is still dominated by *d*-site Fe^{3+}, while in the TbIG layer the Tb^{3+} sublattice overcome the Fe^{3+} sublattices and dominate the overall magnetization. Because the magnetic moments direction of different sublattices have been reversed, the overall magnetization of the EuIG and TbIG layers display an antiparallel alignment.

Based on the above discussion, we can start to analyse the two cases in Fig. 4. When Case A (Fe_{TbIG}-Fe_{EuIG} is ferromagnetically coupled) occurs, the parallel alignment of Fe^{3+} sublattices in both EuIG and TbIG implies that a larger Tb^{3+} moment M_{Tb} is required to balance with the overall Fe^{3+} moments in both TbIG and EuIG layers. Therefore, complete cancellation of M_{Fe} by the (highly temperature dependent) M_{Tb} can only be achieved at lower temperatures, implying a lower T_{comp} with increasing EuIG thickness. The trend of T_{comp} variation with EuIG thickness in Fig. 3(c) supports such an interpretation. Besides, Fig. 4(a) shows the magnetic moment directions of the Re and Fe sublattices in each iron garnet layer. The parallel alignment of Fe^{3+} sublattices in EuIG and TbIG is also consistent with the descriptions in Figs. 4(c) and 4(d). If the Fe^{3+} sublattices were antiferromagnetically coupled across the interface [Case B, Fig. 4(b)], the total magnetization M_{EuIG} would be in antiparallel alignment with M_{TbIG} above T_{comp}, which contradicts the description in Fig. 4(c) and inconsistent with the T_{comp} change shown in Fig. 3(c).

So, the Fe_{TbIG}-Fe_{EuIG} at the interface is ferromagnetically coupled under TbIG/EuIG system with perpendicular magnetic anisotropy structures. Jakob *et al*. also noted on magnetic coupling in YIG/GdIG with in-plane anisotropy [44]. suggesting the rationality of the Case A model [Fig. 4(a)]. Besides, it should be noticed that in our device structure, EuIG (which has not T_{comp} in bulk) is in direct contact with Pt during R_{AHE} measurements, thus providing a more direct proof of coupling in TbIG/EuIG system. The results presented here provide insights on better understanding the influence of adjacent iron garnet layers on the magnetization compensation and spin-Hall transport in garnet films with PMA structures, and would be useful for designing garnet heterostructures for spintronic devices such as magnon valves [29, 46].

4. Conclusions

In summary, different thickness TbIG/EuIG system with tunable compensation temperature was studied. The T_{comp} can be tuned from 218 K (EuIG = 0 nm) to 156 K (EuIG = 20 nm) by changing the thickness of EuIG because of the ferromagnetic coupling of Fe^{3+} sublattices in the two different layers. This study provides an idea for controlling the compensation behavior in spintronic devices, and it would be helpful for designing the magnon valve with multilayer ferromagnetic devices.

Data Availability

The data will be made available on request.

Acknowledgements

This work is supported by the Hong Kong Research Grants Council (Grant No: 15302320), Hong Kong Innovation and Technology Fund (GHP/040/19SZ), the Hong Kong Polytechnic University (ZVWC, CD6U), and the Guangdong Special Support Project (No. 2019BT02X030).

Appendix A. Supplementary data

Supplementary data to this article can be found online.

References

[1] C. Hahn, G. de Loubens, O. Klein, M. Viret, V.V. Naletov, J. Ben Youssef, Comparative measurements of inverse spin Hall effects and magnetoresistance in YIG/Pt and YIG/Ta, Phys. Rev. B 87(17) (2013) 174417. https://doi.org/10.1103/PhysRevB.87.174417.

[2] H. Nakayama, M. Althammer, Y.T. Chen, K. Uchida, Y. Kajiwara, D. Kikuchi, T. Ohtani, S. Geprags, M. Opel, S. Takahashi, R. Gross, G.E. Bauer, S.T. Goennenwein, E. Saitoh, Spin Hall magnetoresistance induced by a nonequilibrium proximity effect, Phys. Rev. Lett. 110(20) (2013) 206601. https://doi.org/10.1103/PhysRevLett.110.206601.

[3] X. Liang, G. Shi, L. Deng, F. Huang, J. Qin, T. Tang, C. Wang, B. Peng, C. Song, L. Bi, Magnetic proximity effect and anomalous Hall effect in $Pt/Y_3Fe_{5-x}Al_xO_{12}$ heterostructures,

Phys. Rev. Appl. 10(2) (2018) 024051. https://doi.org/10.1103/PhysRevApplied.10.024051.

[4] S. Meyer, M. Althammer, S. Geprägs, M. Opel, R. Gross, S.T.B. Goennenwein, Temperature dependent spin transport properties of platinum inferred from spin Hall magnetoresistance measurements, Appl. Phys. Lett. 104(24) (2014) 242411. https://doi.org/10.1063/1.4885086.

[5] A.Z. Arsad, A.W.M. Zuhdi, N.B.y. Ibrahim, M.A. Hannan, Recent advances in yttrium iron garnet films: methodologies, characterization, properties, applications, and bibliometric analysis for future research directions, Appl. Sci. 13(2) (2023) 1218. https://doi.org/10.3390/app13021218.

[6] C.H. Du, H.L. Wang, Y. Pu, T.L. Meyer, P.M. Woodward, F.Y. Yang, P.C. Hammel, Probing the spin pumping mechanism: exchange coupling with exponential decay in $Y_3Fe_5O_{12}$/barrier/Pt heterostructures, Phys. Rev. Lett. 111(24) (2013) 247202. https://doi.org/10.1103/PhysRevLett.111.247202.

[7] F. Yang, P. Chris Hammel, FMR-driven spin pumping in $Y_3Fe_5O_{12}$-based structures, J. Phys. D: Appl. Phys. 51(25) (2018). https://doi.org/10.1088/1361-6463/aac249.

[8] W. Chen, M. Sigrist, D. Manske, Spin Hall effect induced spin transfer through an insulator, Phys. Rev. B 94(10) (2016) 104412. https://doi.org/10.1103/PhysRevB.94.104412.

[9] S. Vélez, A. Bedoya-Pinto, W. Yan, L.E. Hueso, F. Casanova, Competing effects at Pt/YIG interfaces: Spin Hall magnetoresistance, magnon excitations, and magnetic frustration, Phys. Rev. B 94(17) (2016) 174405. https://doi.org/10.1103/PhysRevB.94.174405.

[10] X. Zhou, L. Ma, Z. Shi, W.J. Fan, J.-G. Zheng, R.F.L. Evans, S.M. Zhou, Magnetotransport in metal/insulating-ferromagnet heterostructures: Spin Hall magnetoresistance or magnetic proximity effect, Phys. Rev. B 92(6) (2015) 060402. https://doi.org/10.1103/PhysRevB.92.060402.

[11] M. Li, L. Jin, Z. Zhong, X. Tang, Q. Yang, L. Zhang, H. Zhang, Impact of interfacial chemical state on spin pumping and inverse spin Hall effect in YIG/Pt hybrids, Phys. Rev. B 102(17) (2020) 174435. https://doi.org/10.1103/PhysRevB.102.174435.

[12] R. Das, V. Kalappattil, R. Geng, H. Luong, M. Pham, T. Nguyen, T. Liu, M. Wu, M.H. Phan, H. Srikanth, Enhanced room-temperature spin Seebeck effect in a YIG/C_{60}/Pt

layered heterostructure, AIP Adv. 8(5) (2018) 055906. https://doi.org/10.1063/1.5007233.

[13] N. Okuma, M.R. Masir, A.H. MacDonald, Theory of the spin-Seebeck effect at a topological-insulator/ferromagnetic-insulator interface, Phys. Rev. B 95(16) (2017) 165418. https://doi.org/10.1103/PhysRevB.95.165418.

[14] Y.K. Liu, H.F. Wong, K.K. Lam, K.H. Chan, C.L. Mak, C.W. Leung, Anomalous Hall effect in Pt/$Tb_3Fe_5O_{12}$ heterostructure: Effect of compensation point, J. Magn. Magn. Mater. 468 (2018) 235-240. https://doi.org/10.1016/j.jmmm.2018.08.018.

[15] Y.J. Hong, J.S. Kum, I.B. Shim, C.S. Kim, Spin rotation at compensation point studies of $Tb_3Fe_5O_{12}$ by MÖssbauer spectroscopy, IEEE Trans. Magn. 40(4) (2004) 2808-2810. https://doi.org/10.1109/tmag.2004.832105.

[16] L. Liu, Z. Fan, Z. Chen, Z. Chen, Z. Ye, H. Zheng, Q. Zeng, W. Jia, S. Li, N. Wang, J. Liu, L. Ma, T. Lin, M. Qiu, S. Li, P. Han, J. Shi, H. An, Spin–orbit torques in heavy metal/ferrimagnetic insulator bilayers near compensation, Appl. Phys. Lett. 119(5) (2021) 052401. https://doi.org/10.1063/5.0057741.

[17] Y. Li, D. Zheng, C. Liu, C. Zhang, B. Fang, A. Chen, Y. Ma, A. Manchon, X. Zhang, Current-induced magnetization switching across a nearly room-temperature compensation point in an insulating compensated ferrimagnet, ACS Nano 16(5) (2022) 8181-8189. https://doi.org/10.1021/acsnano.2c01788.

[18] J.J. Bauer, P. Quarterman, A.J. Grutter, B. Khurana, S. Kundu, K.A. Mkhoyan, J.A. Borchers, C.A. Ross, Magnetic proximity effect in magnetic-insulator/heavy-metal heterostructures across the compensation temperature, Phys. Rev. B 104(9) (2021) 094403. https://doi.org/10.1103/PhysRevB.104.094403.

[19] M. Kuila, Z. Hussain, V.R. Reddy, MOKE study of magnetic compensation in polycrystalline gadolinium iron garnet thin film, J. Magn. Magn. Mater. 473 (2019) 458-463. https://doi.org/10.1016/j.jmmm.2018.10.083.

[20] Q. Shao, A. Grutter, Y. Liu, G. Yu, C.-Y. Yang, D.A. Gilbert, E. Arenholz, P. Shafer, X. Che, C. Tang, M. Aldosary, A. Navabi, Q.L. He, B.J. Kirby, J. Shi, K.L. Wang, Exploring interfacial exchange coupling and sublattice effect in heavy metal/ferrimagnetic insulator heterostructures using Hall measurements, x-ray magnetic circular dichroism, and neutron reflectometry, Phys. Rev. B 99(10) (2019) 104401.

https://doi.org/10.1103/PhysRevB.99.104401.

[21] S. Geprags, A. Kehlberger, F.D. Coletta, Z. Qiu, E.J. Guo, T. Schulz, C. Mix, S. Meyer, A. Kamra, M. Althammer, H. Huebl, G. Jakob, Y. Ohnuma, H. Adachi, J. Barker, S. Maekawa, G.E.W. Bauer, E. Saitoh, R. Gross, S.T.B. Goennenwein, M. Klaui, Origin of the spin Seebeck effect in compensated ferrimagnets, Nat. Commun. 7 (2016) 10452. https://doi.org/10.1038/ncomms10452.

[22] A. Chanda, N. Schulz, C. Holzmann, J. Seyd, M. Albrecht, M.-H. Phan, H. Srikanth, Thermal generation of spin current and magnon propagation length in compensated ferrimagnetic $Gd_3Fe_5O_{12}$ thin films, IEEE Trans. Magn. 58(8) (2022) 1-5. https://doi.org/10.1109/tmag.2022.3144835.

[23] J.M. Liang, X.W. Zhao, Y.K. Liu, P.G. Li, S.M. Ng, H.F. Wong, W.F. Cheng, Y. Zhou, J.Y. Dai, C.L. Mak, C.W. Leung, The thickness effect on the compensation temperature of rare-earth garnet thin films, Appl. Phys. Lett. 122(24) (2023) 242401. https://doi.org/10.1063/5.0150228.

[24] H. Chen, D. Cheng, H. Yang, D. Wang, S. Zhou, Z. Shi, X. Qiu, Magnetization switching induced by magnetic field and electric current in perpendicular TbIG/Pt bilayers, Appl. Phys. Lett. 116(11) (2020) 112401. https://doi.org/10.1063/1.5140530.

[25] J.M. Liang, X.W. Zhao, S.M. Ng, H.F. Wong, Y.K. Liu, C.L. Mak, C.W. Leung, Observation of interfacial antiferromagnetic coupling between ferrimagnetic garnet thin films, IEEE Trans. Magn. 58(2) (2022) 1-5. https://doi.org/10.1109/tmag.2021.3087822.

[26] B.W. Dong, J. Cramer, K. Ganzhorn, H.Y. Yuan, E.J. Guo, S.T.B. Goennenwein, M. Klaui, Spin Hall magnetoresistance in the non-collinear ferrimagnet GdIG close to the compensation temperature, J. Phys. Condens. Matter. 30(3) (2018) 035802. https://doi.org/10.1088/1361-648X/aa9e26.

[27] W. Zhang, M.B. Jungfleisch, W. Jiang, Y. Liu, J.E. Pearson, S.G.E.t. Velthuis, A. Hoffmann, F. Freimuth, Y. Mokrousov, Reduced spin-Hall effects from magnetic proximity, Phys. Rev. B 91(11) (2015) 115316. https://doi.org/10.1103/PhysRevB.91.115316.

[28] S. Ding, Z. Liang, C. Yun, R. Wu, M. Xue, Z. Lin, A. Ross, S. Becker, W. Yang, X. Ma, D. Chen, K. Sun, G. Jakob, M. Kläui, J. Yang, Anomalous Hall effect in magnetic

insulator heterostructures: Contributions from spin-Hall and magnetic-proximity effects, Phys. Rev. B 104(22) (2021) 224410. https://doi.org/10.1103/PhysRevB.104.224410.

[29] C.Y. Guo, C.H. Wan, X. Wang, C. Fang, P. Tang, W.J. Kong, M.K. Zhao, L.N. Jiang, B.S. Tao, G.Q. Yu, X.F. Han, Magnon valves based on YIG/NiO/YIG all-insulating magnon junctions, Phys. Rev. B 98(13) (2018) 134426. https://doi.org/10.1103/PhysRevB.98.134426.

[30] Y. Chen, E. Cogulu, D. Roy, J. Ding, J.B. Mohammadi, P.G. Kotula, N.A. Missert, M. Wu, A.D. Kent, Spin transport in an insulating ferrimagnetic-antiferromagnetic-ferrimagnetic trilayer as a function of temperature, AIP Adv. 9(10) (2019) 105319. https://doi.org/10.1063/1.5116549.

[31] S. Mokarian Zanjani, M.C. Onbaşlı, Predicting new iron garnet thin films with perpendicular magnetic anisotropy, J. Magn. Magn. Mater. 499 (2020) 166108. https://doi.org/10.1016/j.jmmm.2019.166108.

[32] H. Fuess, G. Bassi, M. Bonnet, A. Delapalme, Neutron scattering length of terbium structure refinement and magnetic moments of terbium iron garnet, Solid State Commun. 18 (1976) 557. https://doi.org/10.1016/0038-1098(76)91480-0.

[33] V.H. Ortiz, M. Aldosary, J. Li, Y. Xu, M.I. Lohmann, P. Sellappan, Y. Kodera, J.E. Garay, J. Shi, Systematic control of strain-induced perpendicular magnetic anisotropy in epitaxial europium and terbium iron garnet thin films, APL Mater. 6(12) (2018) 121113. https://doi.org/10.1063/1.5078645.

[34] V.H. Ortiz, B. Arkook, J. Li, M. Aldosary, M. Biggerstaff, W. Yuan, C. Warren, Y. Kodera, J.E. Garay, I. Barsukov, J. Shi, First- and second-order magnetic anisotropy and damping of europium iron garnet under high strain, Phys. Rev. Mater. 5(12) (2021) 124414. https://doi.org/10.1103/PhysRevMaterials.5.124414.

[35] C. Tang, P. Sellappan, Y. Liu, Y. Xu, J.E. Garay, J. Shi, Anomalous Hall hysteresis in$Tm_3Fe_5O_{12}$/Pt with strain-induced perpendicular magnetic anisotropy, Phys. Rev. B 94(14) (2016) 140403. https://doi.org/10.1103/PhysRevB.94.140403.

[36] J.J. Bauer, E.R. Rosenberg, C.A. Ross, Perpendicular magnetic anisotropy and spin mixing conductance in polycrystalline europium iron garnet thin films, Appl. Phys. Lett. 114(5) (2019) 052403. https://doi.org/10.1063/1.5074166.

[37] E.R. Rosenberg, L. Beran, C.O. Avci, C. Zeledon, B. Song, C. Gonzalez-Fuentes, J. Mendil, P. Gambardella, M. Veis, C. Garcia, G.S.D. Beach, C.A. Ross, Magnetism and spin transport in rare-earth-rich epitaxial terbium and europium iron garnet films, Phys. Rev. Mater. 2(9) (2018) 094405. https://doi.org/10.1103/PhysRevMaterials.2.094405.

[38] S.M. Suturin, A.M. Korovin, V.E. Bursian, L.V. Lutsev, V. Bourobina, N.L. Yakovlev, M. Montecchi, L. Pasquali, V. Ukleev, A. Vorobiev, A. Devishvili, N.S. Sokolov, Role of gallium diffusion in the formation of a magnetically dead layer at the $Y_3Fe_5O_{12}/Gd_3Ga_5O_{12}$ epitaxial interface, Phys. Rev. Mater. 2(10) (2018) 104404. https://doi.org/10.1103/PhysRevMaterials.2.104404.

[39] J.M. Gomez-Perez, S. Vélez, L. McKenzie-Sell, M. Amado, J. Herrero-Martín, J. López-López, S. Blanco-Canosa, L.E. Hueso, A. Chuvilin, J.W.A. Robinson, F. Casanova, Synthetic antiferromagnetic coupling between ultrathin insulating garnets, Phys. Rev. Appl. 10(4) (2018) 044046. https://doi.org/10.1103/PhysRevApplied.10.044046.

[40] R. Kumar, S.N. Sarangi, D. Samal, Z. Hossain, Positive exchange bias and inverted hysteresis loop in $Y_3Fe_5O_{12}/Gd_3Ga_5O_{12}$, Phys. Rev. B 103(6) (2021) 064421. https://doi.org/10.1103/PhysRevB.103.064421.

[41] M. Uemura, T. Yamagishi, S. Ebisu, S. Chikazawa, S. Nagata, A double peak of the coercive force near the compensation temperature in the rare earth iron garnets, Philos. Mag. 88(2) (2008) 209-228. https://doi.org/10.1080/14786430701805582.

[42] K.J. Kim, S.K. Kim, Y. Hirata, S.H. Oh, T. Tono, D.H. Kim, T. Okuno, W.S. Ham, S. Kim, G. Go, Y. Tserkovnyak, A. Tsukamoto, T. Moriyama, K.J. Lee, T. Ono, Fast domain wall motion in the vicinity of the angular momentum compensation temperature of ferrimagnets, Nat. Mater. 16(12) (2017) 1187-1192. https://doi.org/10.1038/nmat4990.

[43] W.P. Wolf, J.H. Van Vleck, Magnetism of europium garnet, Phys. Rev. 118(6) (1960) 1490-1492. https://doi.org/10.1103/PhysRev.118.1490.

[44] S. Becker, Z. Ren, F. Fuhrmann, A. Ross, S. Lord, S. Ding, R. Wu, J. Yang, J. Miao, M. Kläui, G. Jakob, Magnetic coupling in $Y_3Fe_5O_{12}/Gd_3Fe_5O_{12}$ heterostructures, Phys. Rev. Appl. 16(1) (2021) 014047. https://doi.org/10.1103/PhysRevApplied.16.014047.

[45] Y.F. Li, X.H. Yang, H. Bai, M.Z. Wang, D.S. Cheng, C. Song, Z. Yuan, Y. Liu, Z. Shi, Strain-tunable magnetic compensation temperature of epitaxial Tb3Fe5O12 thin films,

Phys. Rev. B 108(18) (2023) 184403. https://doi.org/ARTN 18440310.1103/PhysRevB.108.184403.

[46] Z. Li, X. Zhang, D. Zhang, B. Liu, H. Meng, J. Xu, Z. Zhong, X. Tang, H. Zhang, L. Jin, Magnetization dynamics in the YIG/Au/YIG magnon valve, APL Mater. 10(2) (2022) 021101. https://doi.org/10.1063/5.0081104.